

## High Resolution Radar Quantitative Precipitation Estimation in the San Francisco Bay Area: Rainfall Monitoring for the Urban Environment

Robert CIFELLI

*Physical Sciences Division, NOAA / Earth System Research Laboratory, Colorado, USA*

V. CHANDRASEKAR

*Cooperative Institute for Research in the Atmosphere, Colorado State University, Colorado, USA*

Haonan CHEN, and Lynn E. JOHNSON

*Physical Sciences Division, NOAA / Earth System Research Laboratory, Colorado, USA  
Cooperative Institute for Research in the Atmosphere, Colorado State University, Colorado, USA*

*(Manuscript received 1 December 2016, in final form 25 November 2017)*

### Abstract

An X-band radar system was deployed in Santa Clara, CA from February through May 2016 to support the National Weather Service in the event of potential flooding during one of the largest El Niños on record and to provide a better understanding of rainfall processes occurring in the Bay Area. The system was also used to provide high-quality precipitation estimation (quantitative precipitation estimation—QPE) for Santa Clara’s urban hydrologic modeling system. Although the Bay Area has coverage from the Next-Generation Weather Radar (NEXRAD) operational radar network, the combination of topographic influences and proximity to a maritime environment provide unique QPE challenges in this urban region. The X-band radar provided high-quality rainfall estimates that performed better than NEXRAD, demonstrating the added value of the X-band system. High-resolution rainfall monitoring systems in urban regions also provide a host of benefits across different sectors of the economy, including flood damage mitigation, water quality, water supply, and transportation.

**Keywords** dual polarization; X-band radar; QPE; flash flood; San Francisco Bay

### 1. Introduction

The San Francisco Bay Area (hereafter referred to as Bay Area) is home to over seven million people, the second largest urban region in California, and the fifth largest population center in the U.S. This region

also supports one of the most prosperous economies in the U.S. (Bay Area Council Economic Institute Report 2012). In early 2016, the Bay Area hosted the National Football League (NFL) Super Bowl, bringing additional people and focusing national attention to the region. Based on the strong El Niño conditions occurring in the winter of 2015–2016, forecasters, water managers, emergency responders, and other agency officials in the Bay Area were worried about the timing of the Super Bowl event and the potential for significant heavy rainfall and flooding with threats

Corresponding author: Haonan Chen, Physical Sciences Division, NOAA Earth System Research Laboratory, 325 Broadway, Boulder, CO 80305, USA  
E-mail: haonan.chen@noaa.gov  
J-stage Advance Published Date: 12 January 2018



to public safety, costly flood damage to infrastructure, negative impacts to water quality (e.g., combined sewer overflows), and major disruptions in transportation. Indeed, a recent report by the State of California's Department of Water Resources has emphasized that the Bay Area is at risk of catastrophic flooding (California Department of Water Resources 2013). Johnson et al. (2015) quantified the benefits associated with improved monitoring and prediction of rainfall for various sectors of the economy in the Bay Area, including flood mitigation, water supply, ecosystem services, recreation, water quality, and transportation (see also Fig. 1). Using available data in the Bay Area, the benefits of an integrated system of high-resolution radars and forecasting tools were estimated to exceed costs by a factor of five on an annual basis (Johnson et al. 2015). It was concluded that the largest portion of the benefits was associated with flood damage mitigation.

Mitigation of the negative impacts associated with heavy rainfall events requires accurate precipitation monitoring (quantitative precipitation estimation—QPE) and prediction to provide forecasters with sufficient understanding of rapidly changing conditions, allowing them to issue appropriate watches and warnings to authorities and the general public. In the Bay Area, the proximity to terrain and maritime conditions as well as the siting of Weather Surveillance Radars-1988 Doppler (WSR-88DP), also known as Next-Generation Weather Radar (NEXRAD), are all challenges in providing accurate, short-term near-surface rainfall estimates. Moreover, there is little to no radar coverage “upstream” over the ocean to monitor ap-

proaching storms (Westrick et al. 1999).

An example of the challenges of NEXRAD radar coverage for QPE over the Bay Area occurred during San Francisco's highest recorded 1-day (24 h) rainfall total on November 5, 1994. The actual rainfall recorded by the official National Weather Service (NWS) rain gauge was 140.7 mm, whereas NEXRAD recorded less than 13 mm (Reynolds 1995). In the past, NWS has relied on commercial TV radar to help fill in the gaps from NEXRAD to provide improved situational awareness of incoming events. However, these radars are not always available when needed, and their calibration and maintenance are not sufficient so that they cannot be relied upon for accurate QPE.

In response to the El Niño conditions and the timing of the Super Bowl event, NOAA's Physical Sciences Division (PSD) in partnership with the Cooperative Institute for Research in the Atmosphere (CIRA) deployed a dual-polarization X-band (wavelength  $\sim 3$  cm) radar to the region to augment NEXRAD coverage and aid in monitoring precipitation for local forecasters and water managers as well as to better understand precipitation processes occurring in this region. This paper describes the radar deployment, methodology for rainfall estimation, distribution of products to end users, and QPE comparisons with NEXRAD demonstrating the added value of the radar system to monitoring rainfall amounts and patterns in the Bay Area urban environment, as well as the impact of the improved rainfall estimation on different sectors of the economy. Section 2 provides an overview of rainfall processes and necessary conditions for flooding in the Bay Area region. Section 3 describes

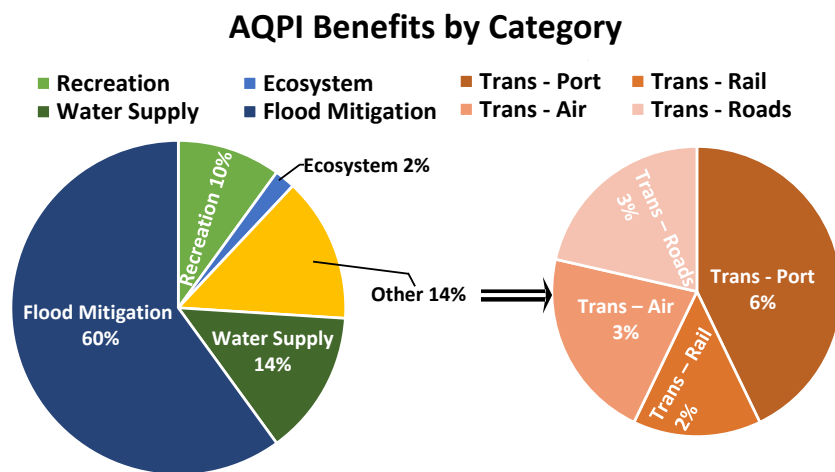


Fig. 1. Characterization of benefits across various economic sectors for an integrated system of high-resolution radars and forecasting tools in the Bay Area (from Johnson et al. 2015).

deployment of the X-band system and generation of rainfall products. Rainfall estimation and the evaluation of QPE procedures are addressed in Section 4. A summary of the results is described in Section 5.

## 2. Synoptic environment and QPE challenges

The Bay Area precipitation climatology, as represented by the NWS Mission Dolores rain gauge in downtown San Francisco (gauge ID 047772), receives about 540 mm of annual precipitation. The precipitation falls predominantly in the cool season as rain, mostly in the five-month period between November and March, and is associated with land-falling extra-tropical cyclones. These cyclones are synoptic-scale and are responsible for replenishing water supply to reservoirs across California and other western states. However, the moisture associated with these systems can also bring heavy rainfall and flooding to the west coast regions, including the Bay Area.

### 2.1 Rainfall characteristics

A number of studies have examined rainfall characteristics in the central California coastal region. White et al. (2003) analyzed airborne radar and vertically pointing precipitation profiler (S-PROF) data during the California Land-Falling Jets (CALJET; Ralph et al. 1998) experiment to show the importance of non-bright band (NBB) rain to total rainfall. NBB rain is described as a shallow collision-coalescence rainfall process where ice microphysics does not play a dominant role. White et al. found that approximately 35 % of the total rainfall was associated with NBB rain<sup>1</sup>. Wind direction and terrain forcing were found to be the primary mechanisms responsible for NBB rain. White et al. (2003) further showed that NBB rain can occur both pre and post cold frontal passage and documented NBB rain rates that can exceed 20 mm h<sup>-1</sup>. This study also showed that NBB rain may preferentially occur in shallow stably stratified flow. Matrosov et al. (2014) studied rainfall characteristics in the Russian River basin, just north of the Bay Area, and reiterated the importance of NBB rain in terms of the overall contribution to rainfall.

To further demonstrate the variability of microphysical characteristics and resulting QPE challenges, raindrop size distribution (DSD) data collected by two NOAA PSD Parsivel disdrometers during the storm season in 2015 were used to derive the median volume

diameter of raindrops (i.e.,  $D_0$ ) and the normalized intercept parameter (i.e.,  $N_w$ ) of the commonly used gamma DSD model (Ulbrich 1983). The disdrometers were deployed in the Russian River watershed: one in Santa Rosa, CA (STR: 122.8022°W, 38.5155°N) over the valley and another at Middletown (MDT: 122.7112°W, 38.7457°N) located in the mountains near the eastern boundary of the watershed (see Fig. 2). The distance between the two disdrometers is 27 km. The elevation of STR and MDT is 32 m above mean sea level (MSL) and 981 m above MSL, respectively. The sampling resolution of both disdrometers was 2 min. Figure 3 shows the distribution of  $D_0$  and  $N_w$  observed by these two disdrometers during the precipitation events in January–February 2015. In this two-month period, there were about 107 rainy hours.

Figure 3 shows different DSD characteristics at these sites. In particular, more small drops (< 0.5 mm) and large drops (> 2 mm) are observed at MDT, whereas more moderate drops (between 0.5 and 2 mm) are observed at STR. Consistent with  $D_0$ , the  $N_w$  plots (Fig. 3b) show a broader distribution of intercept parameter values sampled at MDT, likely due to multiple rainfall processes, compared with the more uniform distribution sampled at STR. The complex DSD characteristics at MDT likely reflect a combination of rainfall processes including bright band rain with robust ice processes and subsequent melting and NBB rain dominated by collision-coalescence below the melting level resulting from orographic enhancement. The results are in agreement with those of Martner et al. (2008), who studied rainfall characteristics in a nearby region using vertically pointing radar data. The differences in DSD characteristics over relatively short distances emphasize the challenge of providing accurate QPE in this complex terrain region.

### 2.2 Heavy rainfall and flooding events in the Bay Area

A number of studies have examined the ingredients responsible for heavy rainfall and flooding events in the Bay Area and other parts of California. Ralph et al. (2003, 2006) showed that flooding was often associated with moisture transport within the warm sector of land-falling extra-tropical cyclones. This meridional water vapor transport often occurs in narrow regions and is commonly referred to as an atmospheric river (AR). Ralph et al. (2003) examined an AR event sampled during CALJET that produced significant flooding in the coastal Santa Cruz Mountains south of the Bay Area. They showed that orographic enhancement and wind direction were key factors determining the

<sup>1</sup> Hybrid rain, which includes some of the properties of NBB rain (namely, low-level collision-coalescence growth), contributed another 44 % to the total rainfall.

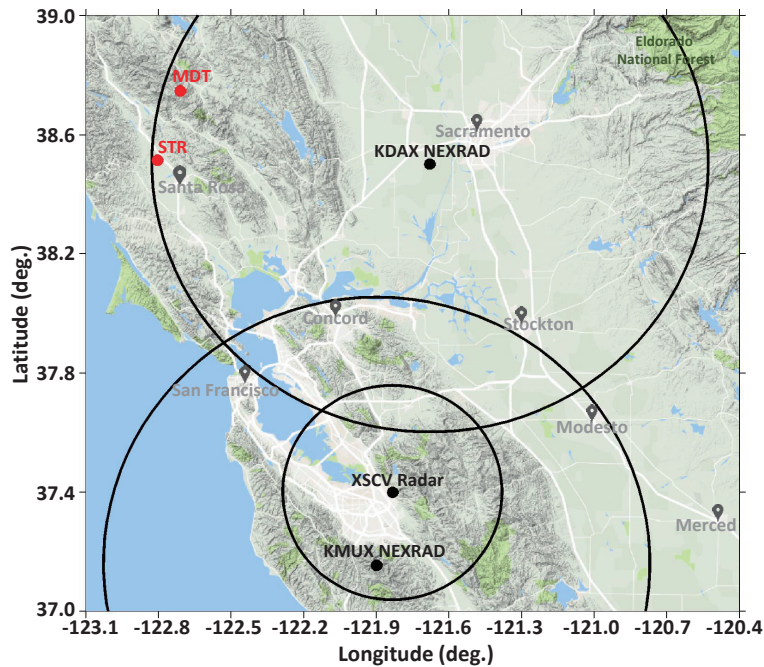


Fig. 2. Map showing the locations of the S-band KMUX and KDAX radars and 100 km coverage rings relative to the Bay Area urban region. The X-band XSCV radar is also shown with its 40 km coverage ring. The disdrometer locations described in Section 2.1 are indicated in red as MDT and STR.

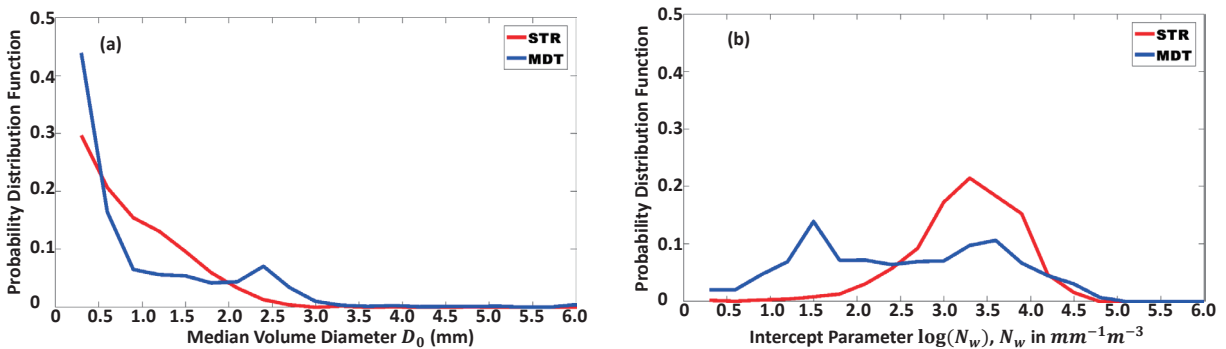


Fig. 3. Distribution of  $D_0$  and  $N_w$  observed by Parsivel disdrometers deployed in Santa Rosa (i.e., STR) and Middletown (i.e., MDT) during the precipitation events in January–February 2015. The locations of these two disdrometers are indicated in Fig. 2. During this two-month period, there were about 107 rainy hours.

extent of heavy rain and resulting flooding impacts. Slight changes in wind direction were shown to produce large changes in rainfall and flooding response.

Ralph et al. (2006) cited the importance of ARs in producing flooding in the Russian River basin. All the events examined in the Ralph et al. study between 1997 and 2005 were associated with ARs. Neiman et al. (2008) used a combination of satellite- and

ground-based data and showed that, at least in California, ARs produce twice as much precipitation as all other storms. The ARs in the Neiman et al. (2008) study were associated with anomalous warm conditions, consistent with the predominant occurrence of these features in the pre-frontal warm sector of the extra-tropical cyclone. This study also showed that, in California, ARs can increase snow water equivalent

(SWE) in the fall–winter seasons and decrease SWE in the spring.

Recent work has shown that ARs can stall as they move onshore, leading to prolonged rainfall and flooding. A study by Blier et al. (2005) described a heavy rainfall event that flooded portions of San Francisco in 2004 associated with a cold front within a land-falling extra-tropical cyclone that stalled over the region. A rain gauge network operated by the City of San Francisco’s Public Utility Commission (PUC) showed that over 38 mm of rain fell within a 30 min period associated with the passage of a narrow cold frontal rainband. The Blier et al. (2005) study documented large precipitation gradients associated with the event that were not well captured in the observations, even with the PUC rain gauge network. Neiman et al. (2016) has shown that mesoscale frontal waves forming along the cold frontal boundary of land-falling extra-tropical cyclones can lead to prolonged periods of AR conditions, enhancing the risk of flooding.

Analysis of PUC rain gauge data for storms occurring during the period October 2004 through March 2005 characterized the variability of rainfall amounts between gauges for a number of rainfall events in the City of San Francisco. Figure 4 shows the coefficient of variability (ratio of the standard deviation to the mean) of hourly rainfall amounts for a winter rainfall season in San Francisco. The gauge data show that rainfall amounts are highly variable from gauge to gauge, especially for the lower hourly accumulations. These low rain intensities ( $< 2.5 \text{ mm h}^{-1}$ ) can be impactful in the City given the highly impervious landscape. The results in Fig. 4 indicate that the PUC gauge network alone cannot adequately resolve the rainfall patterns across the City during many rainfall events.

### 2.3 NEXRAD coverage and impacts on QPE

Westrick et al. (1999) reviewed issues related to the density of the NEXRAD network and minimum scanning elevation angle in many flood-prone watersheds along the west coast of the U.S. The Bay Area is covered by two NEXRADs: KMUX and KDAX (see Fig. 2). However, KMUX is located in the Santa Cruz Mountains at an elevation of over 1000 m compared with the Bay Area urban region which is near sea level. KMUX is also more than 70 km from portions of the Bay Area, including the City of San Francisco. The resulting beam height ( $\sim 2.1 \text{ km AGL}$ ) and width ( $> 1 \text{ km}$ ) are such that this radar cannot be relied upon to accurately resolve precipitation patterns at the urban scale. The KDAX NEXRAD is closer to sea

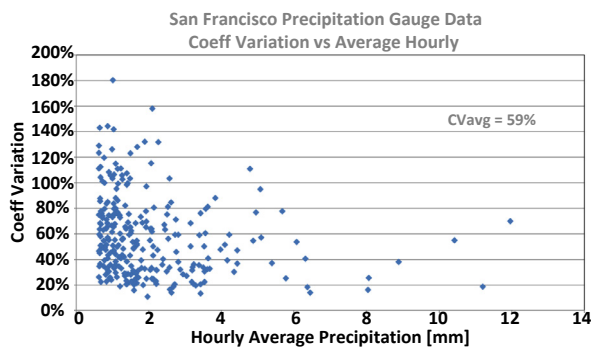


Fig. 4. San Francisco rainfall variability illustrated by computing the coefficient of variability (CV) for hourly rainfall amounts measured by 21 rain gauges operated by the San Francisco PUC. For all events, the average CV is 59%; at higher rainfall amounts ( $> 5.1 \text{ mm h}^{-1}$ ), the residual CV is  $\sim 40\%$ .

level but is located near Davis, CA, over 80 km from the closest portions of the Bay Area. The KDAX radar beam is also partially blocked at low beam elevation angles.

Shortcomings in weather coverage over the offshore region near San Francisco were examined by NOAA using a combination of ground-based and aircraft measurements collected during the late 1990s and early 2000s (Reynolds 1995; White et al. 2003; Matrosov et al. 2005). The shallow NBB rain identified in the White et al. (2003) study was shown to occur below the scanning level of the KMUX NEXRAD. Matrosov et al. (2005) used transportable X-band radar measurements to observe precipitation at low levels that are often missed by NEXRAD. The X-band QPE was focused on the region just offshore and “upstream” of the City of San Francisco and provided detailed precipitation mapping near the surface. Similar to the White et al. study, the Matrosov et al. study showed the importance of shallow rainfall in the region and emphasized that the NEXRAD radar often overshoots or is blocked from detecting these low-level rainfall events. These studies emphasize that, for the Bay Area, radar sampling and analysis strategies tailored to the unique aspects of the urban environment are required.

### 3. X-band deployment and generation of real-time products

In early February of 2016, an X-band dual-polarization radar (hereafter referred to as the XSCV radar) was deployed in Santa Clara Valley at the south end

of the Bay Area. The deployment of this high-resolution radar was a pilot study to evaluate the benefit of improved precipitation monitoring in this region and was a collaboration between NOAA's PSD, CIRA at Colorado State University (CSU), and the Santa Clara Valley Water District (SCVWD). The XSCV radar system specifications and base data products are listed in Table 1. Table 1 also shows the key specifications of a typical NEXRAD system for comparison. Targeted to serve the Super Bowl event, SCVWD officials, NOAA, and CSU crews worked together to have the radar installed and running a few days before the Super Bowl. The radar remained in place through early May 2016 before it was removed. Figure 5a shows the XSCV radar location (latitude: 37.3989°N; longitude: -121.8334°W), its coverage domain, and

its location relative to the KMUX radar. Figure 5a also indicates the rain gauge stations managed by SCVWD. In this study, the rain gauge data are used for cross comparison with the radar-rainfall estimates. The XSCV radar was mounted and placed on the roof of the ozone building at the Penitencia Water Treatment Plant (see Fig. 5b), which is one of the water treatment plants operated by SCVWD in the Santa Clara region. This location provided an unobstructed view of most of the Santa Clara/San Jose urban region, including the Super Bowl stadium. Figure 6 shows the dataflow architecture of the XSCV radar during operation. The radar's servers were housed at the Penitencia Water Treatment Plant. Through Internet and Local Data Manager<sup>2</sup> protocols, the radar data were streamed in real time to CSU and NOAA PSD

Table 1. System specifications of XSCV X-band radar vs. WSR-88DP S-band radar.

	WSR-88DP S-band Radar	XSCV X-band Radar
Transmitter type	Klystron	Magnetron
Center frequency	2.7–3 GHz	9.41 GHz
Peak power	750 kw	8 kw
Average power	1000 w	12 w
Antenna type (diameter)	Front-fed parabolic (9 m)	Front-fed parabolic (1.8 m)
Antenna gain	45.5 dB	41 dB
3-dB beam width	0.95 degree	1.4 degree
Scan speed	Up to 36 deg sec <sup>-1</sup>	Up to 60 deg sec <sup>-1</sup> , 12 deg sec <sup>-1</sup> in the pilot study
Scan acceleration	Up to 17 deg s <sup>-2</sup>	Up to 60 deg s <sup>-2</sup>
Range resolution	1km (250m super resolution)	60 m
Coverage range	230 km	40 km
Update rate	5 ~ 6 minutes	90 seconds
Variables	Level II base data ( $Z$ , $Z_{dr}$ , $V$ , $W$ , $\phi_{dp}$ , $\rho_{hv}$ )	$Z$ , $Z_{dr}$ , $V$ , $W$ , $NCP$ , $\phi_{dp}$ , $K_{dp}$ , $\rho_{hv}$ , and Rain Rate



Fig. 5. (a) Location and coverage map of the X-band dual-polarization XSCV radar in Santa Clara, CA; (b) photo of the XSCV radar during the deployment at the SCVWD Penitencia Water Treatment Plant. The coverage range is 40 km. The red dots in (a) denote the locations of rainfall gauges operated by SCVWD. The blue dot in (a) shows the location of the S-band KMUX NEXRAD radar.

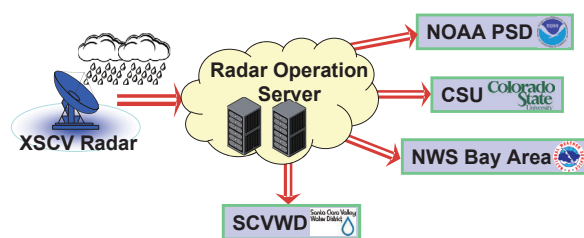


Fig. 6. Dataflow architecture of the X-band dual-polarization XSCV radar.

for data visualization and real-time analysis. The real-time display was available for NOAA PSD, NWS, SCVWD, as well as XSCV radar scientists and engineers at <http://xscv.colostate.edu/>.

In addition, the X-band XSCV radar was in operation during the height of the 2015–2016 El Niño season, and it served as part of the NOAA PSD-led El Niño Rapid Response field campaign (Dole et al. 2017).

During the pilot study, the XSCV radar was set up to conduct effective scanning to ensure high temporal and spatial resolution rainfall products. In particular,  $2^\circ$  and  $3^\circ$  elevation plan position indicator (PPI) sector scans were configured with an update period of 90 s (scan speed  $\sim 12^\circ \text{ s}^{-1}$ ). The PPI sectors were from  $130^\circ$  to  $310^\circ$  in azimuth angle. This sector region was selected primarily based on the orography and population distribution. In particular, this configuration allowed for coverage of most of the densely populated urban regions and commercial districts in the valley southwest of the radar while avoiding the mountain areas northeast of the radar. The latter was desirable in order to reduce the latency and computational complexity caused by signal processing for ground clutter removal.

Figure 7 illustrates the  $2^\circ$  beam heights above MSL as a function of range from the radar for both the S-band KMUX radar and the X-band XSCV radar. The dashed line “A” at 1.1 km height in Fig. 7 corresponds to the altitude of the KMUX radar site, whereas “B” at 0.14 km height represents the altitude of the XSCV radar. The beamwidths of the KMUX and XSCV radar are  $0.95^\circ$  and  $1.4^\circ$ , respectively. Here it should be noted that the 40 km coverage range in Fig. 7 is used only for illustration purposes. In reality, the coverage range of the KMUX NEXRAD radar is 230 km. Figure 7 shows that, even in the south end of

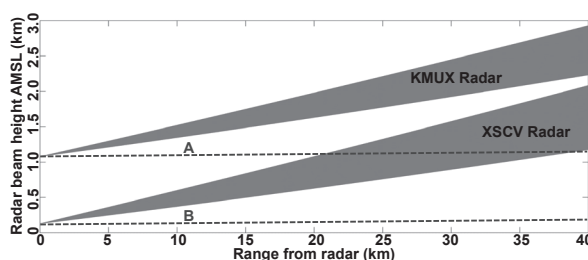


Fig. 7.  $2^\circ$  beam height above MSL as a function of range. The dashed lines “A” (at 1.077 km height) and “B” (at 0.136 km height) represent the altitude (MSL) of the S-band KMUX WSR-88DP radar and the X-band XSCV radar, respectively. The beamwidth of the KMUX radar is  $0.95^\circ$ , and that of the XSCV radar is  $1.4^\circ$ . It should be noted that the coverage range of the KMUX radar is 230 km. The 40 km range is used to illustrate the differences in beam geometry within the range of the XSCV radar.

the Bay Area, most of the lower part ( $< 2$  km) of the atmosphere cannot be sampled by KMUX, and the densely populated San Jose/Santa Clara valley is not well observed due to the high altitude of the KMUX radar site. As a result, high-quality high-resolution rainfall mapping over the valley, especially for the shallow NBB rain scenarios, is challenging. This has been confirmed by previous studies showing that commonly used NEXRAD-based rainfall products often underestimate rainfall in the Bay Area (Matrosov et al. 2014; Willie et al. 2017).

Compared with the scan strategy adopted by NEXRAD (i.e., a repeated volume scan every 5–6 min), the XSCV radar provided higher resolution precipitation information for use in weather forecasts and assisting the water district in their ability to monitor rainfall and streamflow. During the pilot study, the real-time data from  $2^\circ$  scans were used for deriving instantaneous rainfall rate and various rainfall accumulation products. Spatially, the XSCV radar range gate was 60 m. Temporally, the  $2^\circ$  scan update rate was 90 s. For the sake of easy interpretation and for SCVWD’s hydrologic applications, the real-time rainfall rates on radar polar coordinates were mapped onto Cartesian grids with a spatial resolution of  $250 \text{ m} \times 250 \text{ m}$ . This is the resolution used for aggregating running accumulations of rainfall over different time periods, as described below. The real-time rainfall products, stored in ASCII format, were streamed from the radar server to SCVWD (see Fig. 6) to serve as

<sup>2</sup> <https://www.unidata.ucar.edu/software/ldm/>

input to SCVWD's hydrologic model. The rainfall algorithm developed for XSCV radar, as well as the evaluation of various rainfall products, is detailed in the following section.

#### 4. Rainfall algorithm for XSCV radar and performance evaluation

##### 4.1 $K_{dp}$ -based rainfall relation

High-resolution rainfall mapping was one of the main drivers for the deployment of the XSCV X-band dual-polarization radar. It is well known that various rainfall algorithms can be derived based on dual-polarization radar measurements, including reflectivity ( $Z_h$ ), differential reflectivity ( $Z_{dr}$ ), and the specific differential propagation phase ( $K_{dp}$ ) (Cifelli and Chandrasekar 2010). Each rainfall relation has its own advantages and disadvantages, which are attributable to radar operating frequencies and different rain micro-

physical regimes (Bringi and Chandrasekar 2001; Cifelli et al. 2011).

At the X-band, the  $K_{dp}$ -based rainfall relation,  $R = aK_{dp}^b$ , is the only estimator not affected by attenuation (Bringi and Chandrasekar 2001). Chandrasekar et al. (2012) have demonstrated the outstanding performance of  $R(K_{dp})$  for rainfall estimation through a five-year validation study in southwestern Oklahoma. Similarly, Chen and Chandrasekar (2015a) showed the excellent performance of  $R(K_{dp})$  in a relatively flat urban environment. Therefore, we used exclusively the  $K_{dp}$ -based rainfall relation for XSCV radar during this pilot study. In this paper, the methodology proposed by Lim et al. (2014) is implemented to derive the specific parametric form of  $R(K_{dp})$ . This methodology is essentially based on the comparison of rain microphysical signatures between dual-polarization radar observations and simulated DSD data (Lim et al.

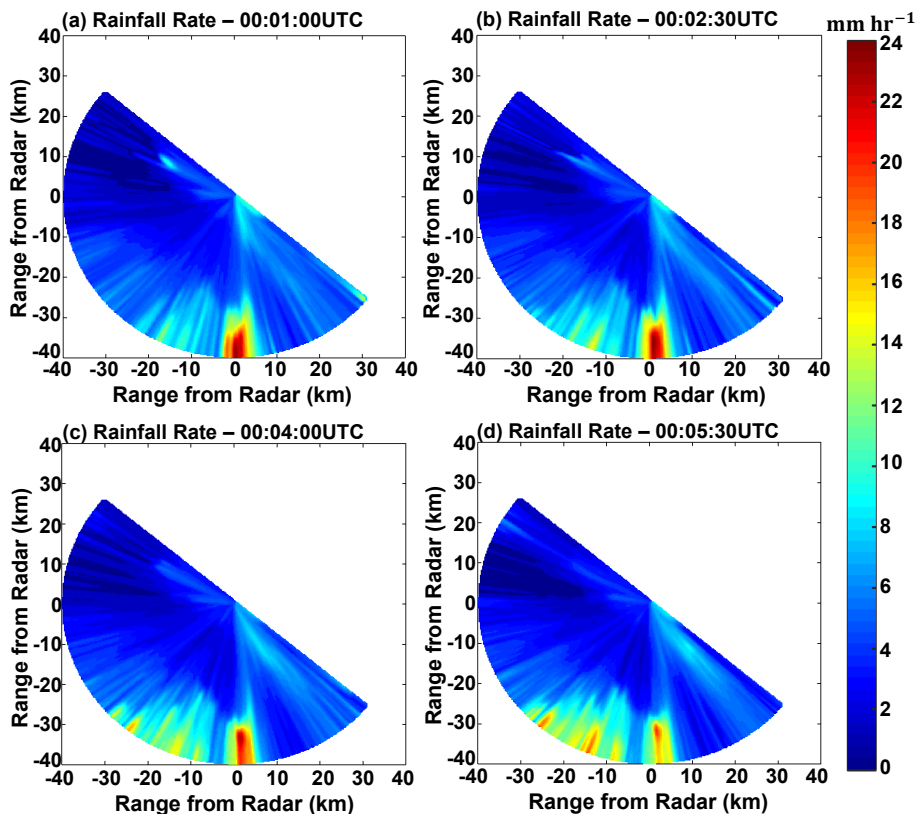


Fig. 8. Consecutive snapshot of  $K_{dp}$ -based rainfall rate from the X-band XSCV radar on March 6, 2016, at (a) 00:01:00 UTC, (b) 00:02:30 UTC, (c) 00:04:00 UTC, and (d) 00:05:30 UTC. The rainfall rates are based on  $2^\circ$  PPI sweeps. The update rate is 90 s. Using the frequently updated  $K_{dp}$ -based rainfall rate field, running accumulations of rainfall at different time intervals are produced in real time, including 15 min, 30 min, 45 min, 60 min, 3 h, and 6 h rainfall amounts (sample products are shown in Fig. 9). The running accumulations of rainfall are also updated every 90 s.

2014). The XSCV radar  $R(K_{dp})$  relation is obtained as

$$R = 20K_{dp}^{0.65}, \quad (1)$$

where  $K_{dp}$  is in  $^{\circ} \text{ km}^{-1}$  and  $R$  is the instantaneous rainfall rate in  $\text{mm h}^{-1}$ .

Figures 8a–d shows consecutive snapshots of the  $R(K_{dp})$ -based rainfall rate from the X-band XSCV radar on March 6, 2016, at 90 s intervals: 00:01:00 UTC, 00:02:30 UTC, 00:04:00 UTC, and 00:05:30 UTC, respectively. The instantaneous rainfall rates are derived based on  $2^{\circ}$  PPI sweeps. With the frequently updated rainfall rate field, running accumulations of rainfall at different time scales are produced in real time, including 15 min, 30 min, 45 min, 60 min, 3 h, and 6 h rainfall amounts. Figure 9 shows sample real-time rainfall accumulation products from the X-band XSCV radar on March 6, 2016. The running accumulations of rainfall are also updated every 90 s.

#### 4.2 Quantitative evaluation of rainfall products

A number of strong winter storms developed in the Bay Area in the late winter–early spring of 2016 after a dry February. In this paper, the storm event that occurred on March 5–7, 2016, was selected in order to demonstrate the rainfall performance of the X-band dual-polarization XSCV radar. This event was associ-

ated with an AR (see Fig. 10) and was well observed passing over the XSCV radar domain. Although this event was characterized mostly by scattered showers and moderate rain rates, the rain was long-lasting, resulting in a major concern of flash flooding. The NWS issued a Flash Flood Watch for the entire Bay Area starting at 22:00 UTC, March 5 and lasting until 06:00 UTC, March 6. Another Flash Flood Watch was issued for the entire Bay Area from 02:00 UTC until 12:00 UTC, March 7. Power outages occurred in some parts of the Peninsula on the west side of the Bay. Widespread stratiform rain moved into the XSCV radar coverage domain around 00 UTC on March 6, 2016, and lasted many hours before it dissipated around 14:00 UTC. Therefore, the XSCV radar data collected during this period are used for QPE evaluation.

To evaluate the performance of rainfall products from the XSCV radar, rainfall records from a network of tipping-bucket rain gauges were used for cross comparison. The gauge network, managed and maintained by SCVWD, consisted of 46 gauge stations. The gauge locations are shown in Fig. 5a. In particular, 30 gauge sites are deployed under the XSCV radar scan domain, which are used for radar rainfall evaluation in this paper. At each gauge station, rainfall data are archived based on the ALERT (Automated Local Evaluation in Real Time) transmission system.

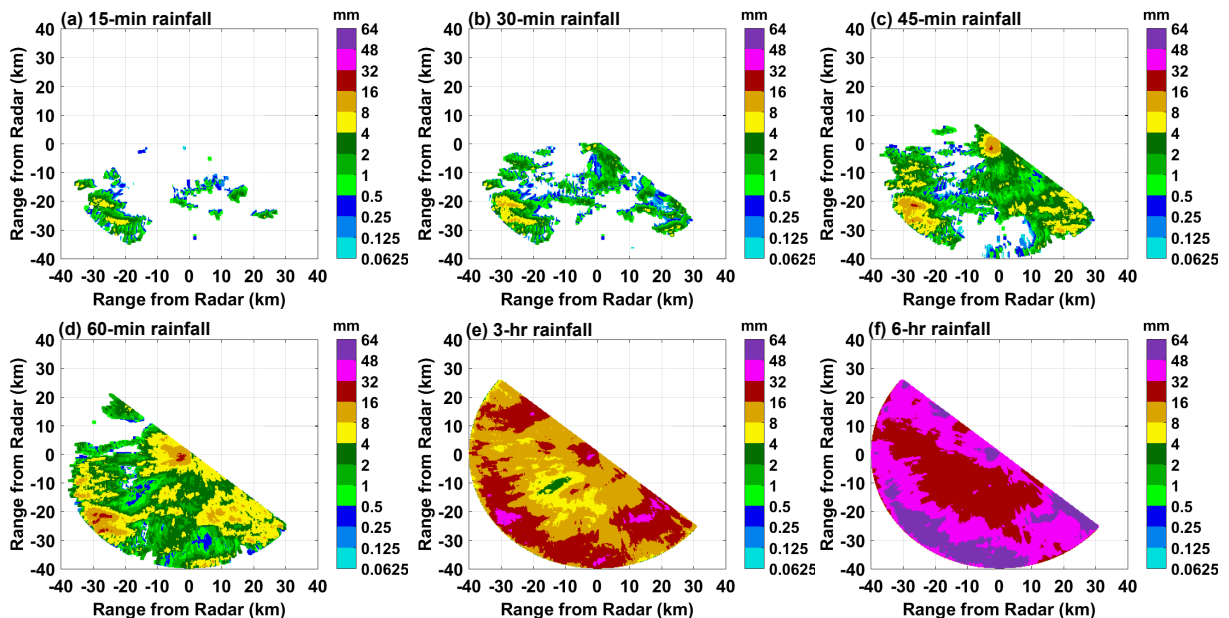


Fig. 9. Sample rainfall accumulation products from the X-band XSCV radar on March 6, 2016, ending at 10:00UTC: (a) 15 min, (b) 30 min, (c) 45 min, (d) 60 min, (e) 3 h, and (f) 6 h rainfall accumulation. The products are based on  $2^{\circ}$  sweeps updated every 90 s.

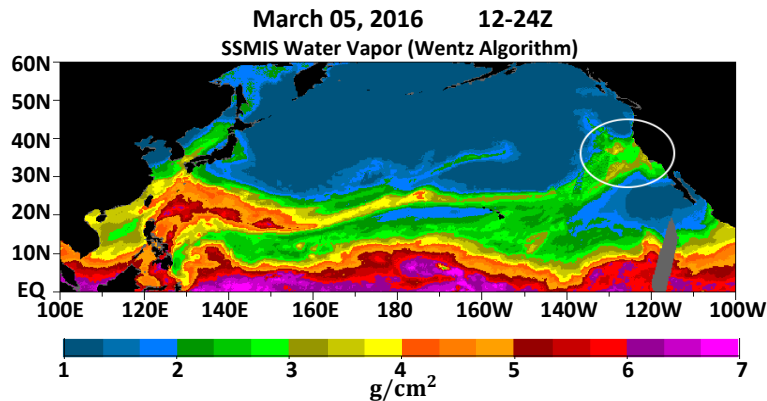


Fig. 10. Integrated water vapor for March 5, 2016. The white circle indicates the AR plume impinging on central California. Note that the satellite retrieval method of integrated water vapor is valid only over ocean regions. Image courtesy of NOAA PSD.

Spatially, the rain gauges provide rainfall measurements at point locations. Temporally, each time 1 mm of rainfall occurs, the information is transmitted to the base station and the data are stored to the nearest second. The rainfall data are then accumulated in 15 min intervals with a resolution of 1 mm. Hence, for the sake of comparison, the estimated XSCV radar rainfall rates (updated every 90 s) within a 15 min window corresponding to the gauge rainfall observation time are used to produce matched radar rainfall amounts. The XSCV grid products at the gauge locations were selected to create radar–gauge rainfall pairs for quantitative evaluation. In addition, 30, 45, and 60 min rainfall accumulations were computed based on the 15 min rainfall estimates from the gauges and XSCV radar.

Figure 11 shows an example cross comparison of rainfall from the XSCV radar and rain gauge 2065 on March 6, 2016. It can be seen that rainfall estimates from the XSCV radar agree well with the gauge observations at all accumulation times. The largest differences occur in the 15 min accumulation time series (Fig. 11a) and reflect the relatively coarse resolution of the gauge (1 mm) combined with the occurrence of low rain intensities. The comparisons at other gauge locations are not shown because they show essentially similar results.

For quantitative comparison of the radar and gauge estimates, a number of metrics were computed, including normalized bias ( $NB$ ), normalized mean absolute error ( $NMAE$ ), and Pearson correlation coefficient ( $CORR$ ), respectively defined as follows:

$$NB = \frac{\langle R_R - R_G \rangle}{\langle R_G \rangle}, \quad (2a)$$

$$NMAE = \frac{\langle |R_R - R_G| \rangle}{\langle R_G \rangle}, \quad (2b)$$

$$CORR = \frac{(R_R - \langle R_R \rangle)(R_G - \langle R_G \rangle)}{\sqrt{\sum (R_R - \langle R_R \rangle)^2} \sqrt{\sum (R_G - \langle R_G \rangle)^2}}, \quad (2c)$$

where  $NB$ ,  $NMAE$ , and  $CORR$  are unitless,  $R_R$  and  $R_G$  denote rainfall accumulations from the radar and rain gauge, respectively, and the angle brackets represent a sample average.

The overall scores based on the rainfall estimates at 30 gauge locations are listed in Table 2. These scores show improvement over previous studies from NEXRAD-based QPE in the Bay Area characterized by complex terrain (e.g., Matrosov et al. 2014; Willie et al. 2017).

It should be emphasized that the rain gauge data are used only for reference to assess relative QPE performance and are not assumed to be “ground truth”. Based on personal communication with SCVWD staff, the rain gauge network is well maintained; however, a detailed analysis of gauge error characteristics was not performed. We further note that the error scores in Table 2 relative to previous X-band studies may be affected by the coarse resolution (1 mm) of the gauge data as noted above, especially at short rainfall integration time intervals during light to moderate rain when it may take too long for the gauge to tip. The interested reader is referred to Chen and Chandrasekar

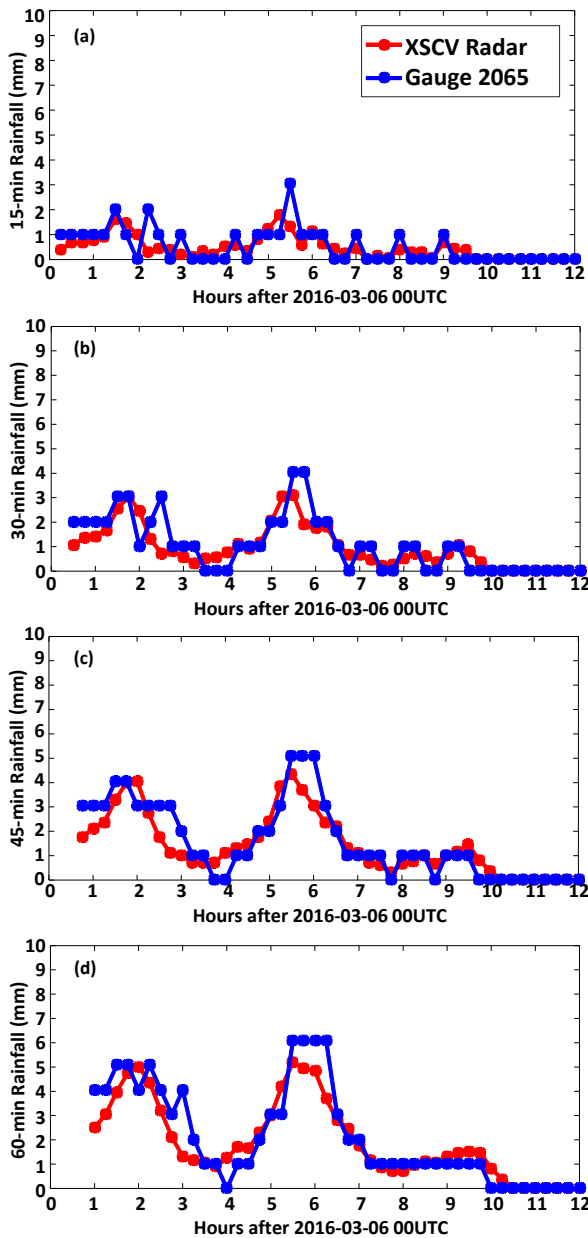


Fig. 11. Cross comparison of rainfall accumulation from the XSCV radar and the SCVWD rain gauge 2065 (37.2383°N, -121.8692°W) on March 6, 2016: (a) 15 min, (b) 30 min, (c) 45 min, and (d) 60 min rainfall accumulation.

(2015b) for the limitations on sampling time and bucket volume resolution, particularly in light rainfall cases.

Table 2. Evaluation results of XSCV radar rainfall products for the rainfall event on March 06, 2016, including the normalized bias (*NB*), normalized mean absolute error (*NMAE*), and Pearson correlation coefficient (*CORR*).

Rainfall Products	NB (%)	NMAE (%)	CORR
15-min rainfall	-6.16	51.58	0.72
30-min rainfall	6.94	37.30	0.80
45-min rainfall	-6.68	35.91	0.76
60-min rainfall	-4.10	35.09	0.86

### 4.3 Cross comparison with NEXRAD-based products

For a side-by-side peer comparison, the rainfall products generated by the NWS for the S-band KMUX NEXRAD radar (both single- and dual-polarization products), as well as the radar-only-based products from the Multi-Radar Multi-Sensor (MRMS) system, are also included in this validation study to place the results in context with operationally available QPE. The NWS single-polarization rainfall algorithm (NEXRAD SP) is presented in Fulton et al. (1998), and the dual-polarization rainfall algorithm (NEXRAD DP) is described in Giangrande and Ryzhkov (2008). Both algorithms generate hourly rainfall accumulations on a polar grid centered at the radar and are available from the National Climatic Data Center. The MRMS system, developed by the National Severe Storms Laboratory (Zhang et al. 2011), also produces hourly rainfall data, but at 1 km × 1 km Cartesian grids. The MRMS radar-only product is used in order to directly compare with XSCV. In this section, the hourly rainfall products based on NEXRAD SP, DP, and MRMS at each gauge location from 00:00 to 13:00 UTC, March 6, 2016, at the location of gauge 1511 (37.3075°N, -121.9950°W), and Fig. 12a illustrates the hourly rainfall at the top of every hour from 00:00 to 13:00 UTC, March 6, 2016, at the location of gauge 1511 (37.3075°N, -121.9950°W), and Fig. 12b shows the rainfall accumulations based on the hourly rainfall estimates in (a). The XSCV radar agrees very well with the gauge rainfall observations. The NEXRAD SP, DP, and MRMS products are underestimating rainfall for this particular event. The overall evaluation scores based on hourly rainfall estimates at the 30 validation gauge locations are shown in Fig. 13. Among the various rainfall products, the XSCV radar-based estimates have the best performance in terms of *NB*, *NMAE*, and *CORR*. The evaluation statistics for the rainfall products at shorter integration time scales are not included because they are not available from either the NEXRAD SP and DP or MRMS.

Comparisons of hourly rainfall were explored

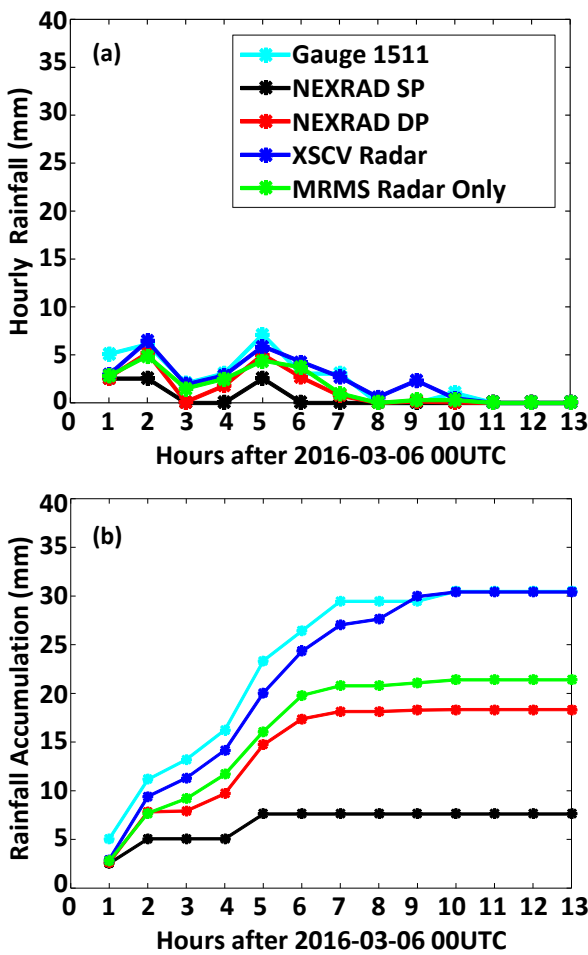


Fig. 12. (a) Hourly rainfall at the top of every hour from 00:00 to 13:00 UTC, March 6, 2016, at the location of the SCVWD rain gauge 1511 (37.3075°N, -121.9950°W); (b) rainfall accumulations based on the hourly estimates shown in (a).

Fig. 14. (a) Probability distribution of hourly rainfall amounts; (b) peak hourly rainfall at the top of every hour from 01:00 to 13:00 UTC, March 6, 2016. The data are based on radar and gauge rainfall observations at 30 gauge locations covered by the XSCV radar.

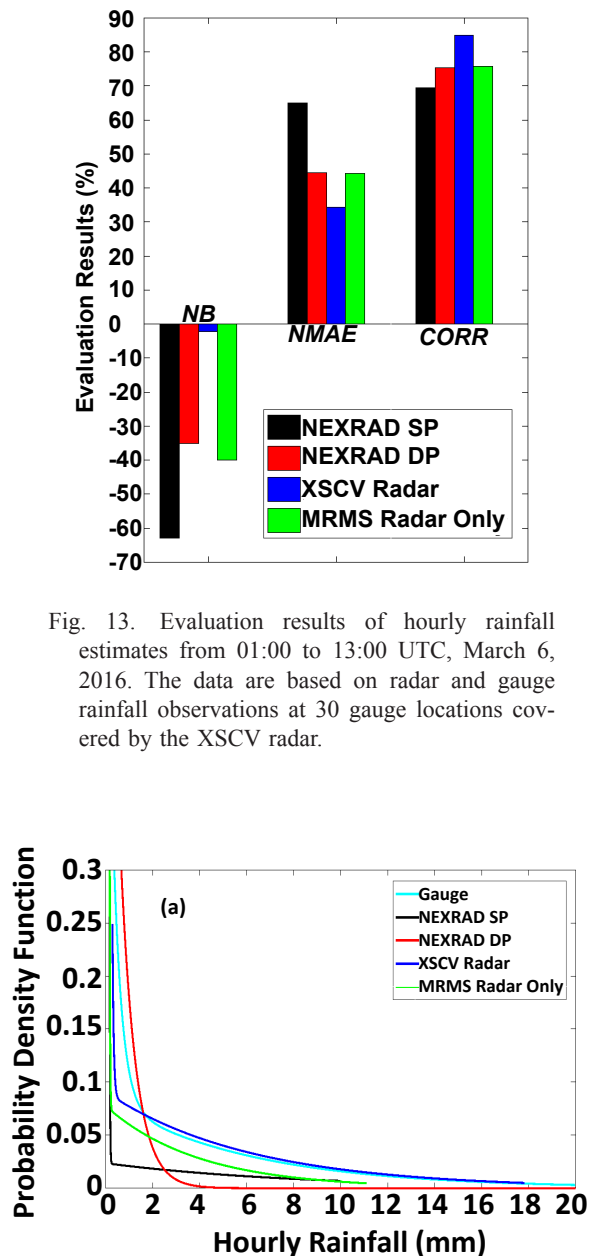


Fig. 13. Evaluation results of hourly rainfall estimates from 01:00 to 13:00 UTC, March 6, 2016. The data are based on radar and gauge rainfall observations at 30 gauge locations covered by the XSCV radar.

Fig. 14. (a) Probability distribution of hourly rainfall amounts; (b) peak hourly rainfall at the top of every hour from 01:00 to 13:00 UTC, March 6, 2016. The data are based on radar and gauge rainfall observations at 30 gauge locations covered by the XSCV radar.

in more detail to better understand the behavior of the different rainfall products over the spectrum of rainfall intensities. The probability distributions of the hourly rainfall estimates are shown in Fig. 14a. With the exception of the lowest rainfall intensities, XSCV matches the gauge rainfall distribution remarkably well. Note that the highest hourly rainfall rates are not even detected by either the NEXRAD SP and DP or MRMS products. The peak hourly rainfall estimates from the NEXRAD-based algorithms, XSCV, and the validation gauges are shown in Fig. 14b. Again, the XSCV-based product has the best performance in terms of identifying the peak rainfall values. Although infrequent, the high rain intensity results shown in Fig. 14 are extremely important for urban flash flood applications.

To further demonstrate the advantages of high-reso-

lution rainfall products from the X-band XSCV radar, rainfall totals during this 13 h period are computed under the XSCV radar coverage domain. The 13 h rainfall accumulations from XSCV radar, MRMS, and another commonly used NWS operational system (i.e., the Multi-Sensor Precipitation Estimator—MPE; Lawrence et al. 2003) are shown in Fig. 15. The MPE system, which is widely used by NWS River Forecast Centers, produces hourly rainfall estimates at the Hydrologic Rainfall Analysis Project resolution, about 4 km × 4 km. Figure 15 illustrates two important points about the XSCV vs MPE or MRMS QPE estimates. First, XSCV shows significantly more accumulated precipitation than either of the NEXRAD-based QPEs. This is especially true in the higher terrain southwest of the San Jose–Santa Clara urban region. The differences may reflect a contribution of shallow

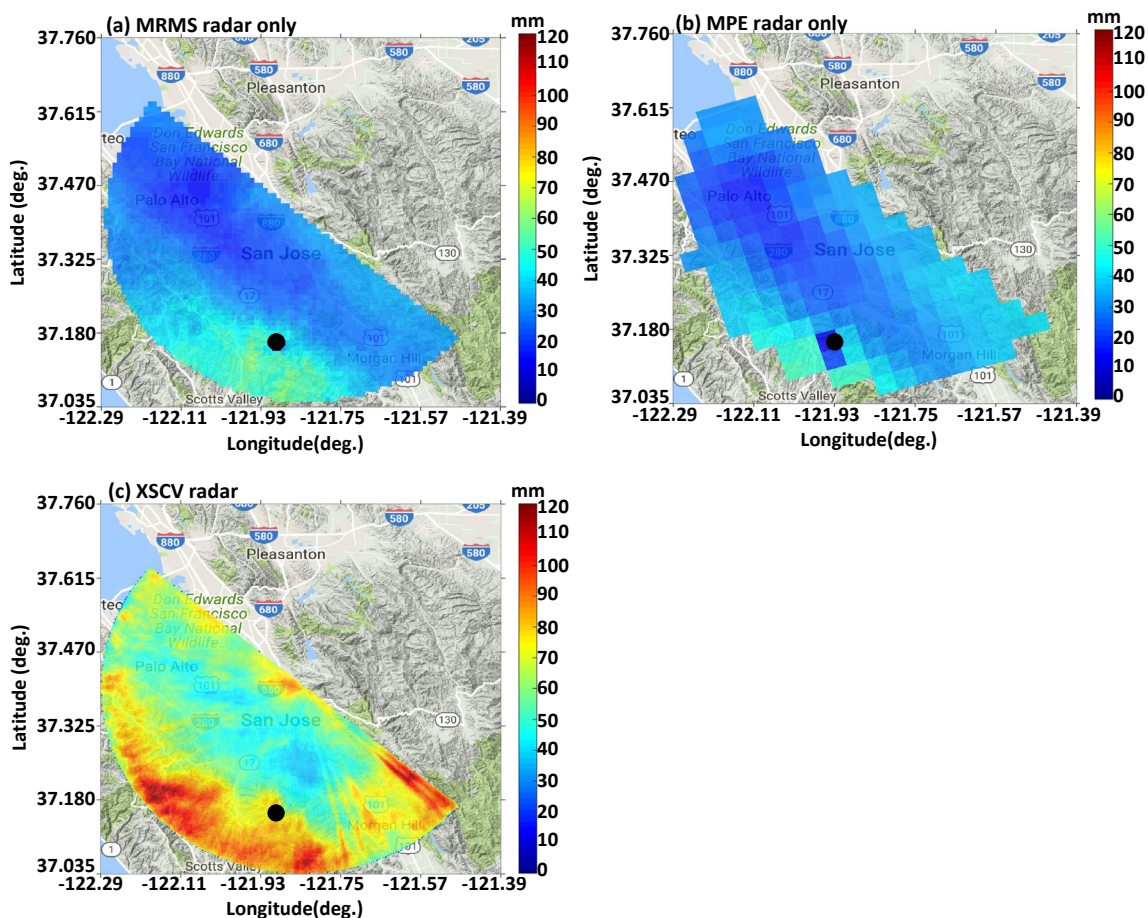


Fig. 15. Radar-rainfall accumulation maps from 00:00 to 13:00 UTC, March 6, 2016: (a) MRMS; (b) MPE; (c) XSCV. The black circle in each panel shows the location of the KMUX NEXRAD. The maps in (a), (b), and (c) were generated using only radar data; no gauge bias correction was applied.

NBB rainfall along the east slope of the Santa Cruz Mountains that is not well observed by the KMUX NEXRAD. The higher values observed by XSCV are in better agreement with the gauge network amounts (e.g., Figs. 11, 12). Second, compared with either MRMS or MPE NEXRAD-based systems, the XSCV radar is able to capture much more detail about the precipitation pattern due to its high resolution. For urban applications, especially highly localized flash flooding, such high-resolution rainfall products are essential for accurate hydrologic prediction.

## 5. Summary

This study described the deployment of an X-band radar in the Bay Area during the winter and spring of 2016. The radar was deployed in response to the strong El Niño conditions coinciding with the hosting of the NFL Super Bowl in the region. The radar also provided a unique pilot study opportunity to examine the benefits of enhanced radar coverage in this region. The radar provided real-time updates of rainfall occurring in the Santa Clara region at the south part of the Bay, which were used by both the NWS and the SCVWD. The radar was deployed to augment NEXRAD coverage and to better understand rainfall processes occurring in the region. The X-band operated at high resolution compared with NEXRAD, providing 90 s updates with 250 m spatial resolution. Although Santa Clara and most of the Bay Area are within the coverage of NEXRAD, the Bay Area is located near sea level, well below the elevation of the KMUX NEXRAD radar site (~1000 m). As such, NEXRAD often misses low-level rainfall in the region. The accuracy of the X-band rainfall estimates was better in comparison to an ALERT rain gauge network operated by the City of Santa Clara. The radar performed better than NEXRAD, especially at the high-end rain rates that are critical for accurate flooding prediction.

This study highlights the importance of high-resolution radar measurements in the urban environment where the hydrologic response time (time to concentration) is relatively short. Improved situational awareness and high-quality QPE provided by the X-band can help inform forecasters of urban flash flood threats and water managers of potential water quality issues resulting from a particular rainfall event. Recent studies have demonstrated the benefits of advanced precipitation monitoring in selected urban regions, including the Bay Area. In particular, a network of X-band radars, sited around San Francisco Bay, could augment the existing NEXRAD coverage

with high-resolution QPE and short-term forecasts and provide a host of benefits across a number of economic sectors, including flood damage mitigation, water quality, and transportation.

## Acknowledgments

NOAA's Office of Oceanic and Atmospheric Research and the Santa Clara Valley Water District (SCVWD) provided support for the Santa Clara radar deployment. The research analysis was supported by the Physical Sciences Division (PSD) at NOAA's Earth System Research Laboratory. The Sonoma County Water Agency provided support for the disdrometer data collection in the Russian River watershed. Tim Coleman and Dan Gottas at PSD QC'd and processed the disdrometer data.

## References

- Bay Area Council Economic Institute, 2012: *The Bay Area: A regional economic assessment*. Bay Area Council Economic Institute report. Bay Area Council Economic Institute, San Francisco, CA, USA, 68 pp.
- Blier, W., J. P. Monteverdi, and J. Null, 2005: The Historic San Francisco flash flood event of 25 February 2004. Preprints, *Sixth Conf. on Coastal Atmospheric and Oceanic Processes*, Amer. Meteor. Soc., San Diego, CA, CD-ROM, 6.
- Bringi, V. N., and V. Chandrasekar, 2001: *Polarimetric Doppler Weather Radar: Principles and Applications*. Cambridge University Press, 636 pp.
- California Department of Water Resources, 2013: *California's flood future: Recommendations for managing the State's flood risk*. State of California Natural Resources Agency Department of Water Resources and the Army Corps of Engineers Flood Plain Management Services Program, 152 pp.
- Chandrasekar, V., Y. Wang, and H. Chen, 2012: The CASA quantitative precipitation estimation system: A five year validation study. *Nat. Hazards Earth Syst. Sci.*, **12**, 2811–2820.
- Chen, H., and V. Chandrasekar, 2015a: The quantitative precipitation estimation system for Dallas-Fort Worth (DFW) urban remote sensing network. *J. Hydrol.*, **531**, 259–271.
- Chen, H., and V. Chandrasekar, 2015b: Estimation of light rainfall using Ku-band dual-polarization radar. *IEEE Trans. Geosci. Remote Sens.*, **53**, 5197–5208.
- Cifelli, R., and V. Chandrasekar, 2010: Dual-polarization radar rainfall estimation. *Rainfall: State of the Science*. Testik, F. Y., and M. Gebremichael (eds.), American Geophysical Union, Washington, DC, 105–125.
- Cifelli, R., V. Chandrasekar, S. Lim, P. C. Kennedy, Y. Wang, and S. A. Rutledge, 2011: A new dual-polarization radar rainfall algorithm: Application in Colorado precipitation events. *J. Atmos. Oceanic Technol.*, **28**, 352–364.
- Dole, R., J. Spackman, M. Newman, G. Compo, C. Smith, L. Hartten, J. Barsugli, R. Webb, M. Hoerling, R.

- Cifelli, K., Wolter, C., Barnett, M., Gehne, R., Gelaro, G., Kiladis, S., Abbott, J., Albers, J., Brown, C., Cox, L., Darby, G., de Boer, B., DeLuisi, J., Dias, J., Dunion, J., Eischeid, C., Fairall, A., Gambacorta, B., Gorton, A., Hoell, J., Intrieri, D., Jackson, P., Johnston, E., Akish, R., Lataitis, K., Mahoney, K., McCaffrey, H., Alex McColl, M., Mueller, D., Murray, P., Neiman, W., Otto, O., Persson, X., Quan, I., Rangwala, A., Ray, D., Reynolds, E., Riley Dellaripa, K., Rosenlof, N., Sakaeda, P., Sardeshmukh, L., Slivinski, A., Solomon, L., Smith, D., Swales, S., Tulich, A., White, G., Wick, M., Winterkorn, D., Wolfe, and R. Zamora, 2017: Advancing science and services during the 2015–16 El Niño: The NOAA El Niño rapid response field campaign. *Bull. Amer. Meteor. Soc.*, doi:10.1175/BAMS-D-16-0219.1, in press.
- Fulton, R. A., J. P. Breidenbach, D.-J. Seo, D. A. Miller, and T. O'Bannon, 1998: The WSR-88D rainfall algorithm. *Wea. Forecasting*, **13**, 377–395.
- Giangrande, S. E., and A. V. Ryzhkov, 2008: Estimation of rainfall based on the results of polarimetric echo classification. *J. Appl. Meteor. Climatol.*, **47**, 2445–2462.
- Johnson, L. E., R. Cifelli, and A. B. White, 2015: *Benefits of an advanced quantitative precipitation information system: San Francisco Bay Area case study*. NOAA Technical Memorandum OAR PSD-315, 59 pp., doi: 10.7289/V5WS8R6X.
- Lawrence, B. A., M. I. Shebsovich, M. J. Glaudemans, and P. S. Tilles, 2003: Enhancing precipitation estimation capabilities at National Weather Service field offices using multi-sensor precipitation data mosaics. Preprints, *19th International Conference on Interactive Information Processing Systems for Meteorology, Oceanography and Hydrology*, Amer. Meteor. Soc., Long Beach, California.
- Lim, S., H. Chen, K.-H. Lee, and B.-J. Jang, 2014: Rain microphysical properties based on radar observation in Korea. *Proc. of the XXXIth URSI General Assembly and Scientific Symposium (URSI GASS)*, IEEE, Beijing, China, 1–2, doi:10.1109/URSIGASS.2014.6929642.
- Martner, B. E., S. E. Yuter, A. B. White, S. Y. Matrosov, D. E. Kingsmill, and F. M. Ralph, 2008: Raindrop size distributions and rain characteristics in California coastal rainfall for periods with and without a radar bright band. *J. Hydrometeorol.*, **9**, 408–425.
- Matrosov, S. Y., D. E. Kingsmill, B. E. Martner, and F. M. Ralph, 2005: The utility of X-band polarimetric radar for continuous quantitative estimates of rainfall parameters. *J. Hydrometeorol.*, **6**, 248–262.
- Matrosov, S. Y., F. M. Ralph, P. J. Neiman, and A. B. White, 2014: Quantitative assessment of operational weather radar rainfall estimates over California's northern Sonoma County using HMT-West data. *J. Hydrometeorol.*, **15**, 393–410.
- Neiman, P. J., F. M. Ralph, G. A. Wick, J. D. Lundquist, and M. D. Dettinger, 2008: Meteorological characteristics and overland precipitation impacts of atmospheric rivers affecting the West Coast of North America based on eight years of SSM/I satellite observations. *J. Hydrometeorol.*, **9**, 22–47.
- Neiman, P. J., B. J. Moore, A. B. White, G. A. Wick, J. Aikins, D. L. Jackson, J. R. Spackman, and F. M. Ralph, 2016: An airborne and ground-based study of a long-lived and intense atmospheric river with mesoscale frontal waves impacting California during CalWater-2014. *Mon. Wea. Rev.*, **144**, 1115–1144.
- Ralph, F. M., P. O. Persson, D. Reynolds, P. J. Neiman, W. Nuss, J. Schmidt, D. Jorgensen, C. King, A. White, J. Bao, and W. Neff, 1998: The use of tropospheric profiling in the California Land-Falling Jets Experiment (CALJET). *Proceedings of 4th Symposium on Tropospheric Profiling, Needs and Technologies*, University of Colorado, Aspen, CO, 258–260.
- Ralph, F. M., P. J. Neiman, D. E. Kingsmill, P. O. G. Persson, A. B. White, E. T. Strem, E. D. Andrews, and R. C. Antweiler, 2003: The impact of a prominent rain shadow on flooding in California's Santa Cruz Mountains: A CALJET case study and sensitivity to the ENSO cycle. *J. Hydrometeorol.*, **4**, 1243–1264.
- Ralph, F. M., P. J. Neiman, G. A. Wick, S. I. Gutman, M. D. Dettinger, D. R. Cayan, and A. B. White, 2006: Flooding on California's Russian River: Role of atmospheric rivers. *Geophys. Res. Lett.*, **33**, L13801, doi: 10.1029/2006GL026689.
- Reynolds, D. W., 1995: *Warm rain process and WSR-88D*. Western Region Tech. Attachment, No.95–08, 7 pp.
- Ulbrich, C. W., 1983: Natural variations in the analytical form of the raindrop size distribution. *J. Climate Appl. Meteorol.*, **22**, 1764–1775.
- Westrick, K. J., C. F. Mass, and B. A. Colle, 1999: The limitations of the WSR-88D radar network for quantitative precipitation measurement over the coastal western United States. *Bull. Amer. Meteor. Soc.*, **80**, 2289–2298.
- White, A. B., P. J. Neiman, F. M. Ralph, D. E. Kingsmill, and P. O. G. Persson, 2003: Coastal orographic rainfall processes observed by radar during the California Land-Falling Jets Experiment. *J. Hydrometeorol.*, **4**, 264–282.
- Willie, D., H. Chen, V. Chandrasekar, R. Cifelli, C. Campbell, D. Reynolds, S. Matrosov, and Y. Zhang, 2017: Evaluation of multisensor quantitative precipitation estimation in Russian River basin. *J. Hydrol. Eng.*, **22**, E5016002, doi:10.1061/(ASCE)HE.1943-5584.0001422.
- Zhang, J., K. Howard, C. Langston, S. Vasiloff, B. Kaney, A. Arthur, S. Van Cooten, K. Kelleher, D. Kitzmiller, F. Ding, D.-J. Seo, E. Wells, and C. Dempsey, 2011: National Mosaic and Multi-sensor QPE (NMQ) system: Description, results, and future plans. *Bull. Amer. Meteor. Soc.*, **92**, 1321–1338.